HHS Public Access

Author manuscript

Stem Cells. Author manuscript; available in PMC 2020 April 01.

Published in final edited form as:

Stem Cells. 2019 April ; 37(4): 555–567. doi:10.1002/stem.2970.

Hypoxia Prevents Mitochondrial Dysfunction and Senescence in Human c-Kit+ Cardiac Progenitor Cells

Kelli I. Korski[*,1], **Dieter A. Kubli**[*,1], **Bingyan J. Wang**[1], **Farid G. Khalafalla**[1], **Megan M. Monsanto**[1], **Fareheh Firouzi**[1], **Oscar H. Echeagaray**[1], **Taeyong Kim**[1], **Robert M. Adamson**[2], **Walter P. Dembitsky**[2], **Åsa B. Gustafsson**[3], and **Mark A. Sussman**[1,**]

[1]San Diego State University, Department of Biology and Integrated Regenerative Research Institute, San Diego, California.

[2]Division of Cardiology, Sharp Hospital, San Diego, CA

[3]The Skaggs School of Pharmacy and Pharmaceutical Sciences, Department of Pharmacology, University of California San Diego, La Jolla

Abstract

Senescence-associated dysfunction deleteriously affects biological activites of human c-Kit+ cardiac progenitor cells (hCPCs), particularly under conditions of *in vitro* culture. In comparison, preservation of self-renewal and decreases in mitochondrial reactive oxygen species (ROS) are characteristic of murine CPCs *in vivo* that reside within hypoxic niches. Recapitulating hypoxic niche oxygen tension conditions of ~1% O_2 *in vitro* for expansion of hCPCs rather than typical normoxic cell culture conditions (21% O_2) could provide significant improvement of functional and biological activity of hCPCs. hCPCs were isolated and expanded under permanent hypoxia (hCPC-1%) or normoxia (hCPC-21%) from left ventricular tissue explants collected during left ventricular assist device implantation. hCPC-1% exhibit increased self-renewal and suppression of senescence characteristics relative to hCPC-21%. Oxidative stress contributed to higher susceptibility to apoptosis, as well as decreased mitochondrial function in hCPC-21%. Hypoxia prevented accumulation of dysfunctional mitochondria, supporting higher oxygen consumption rates and mitochondrial membrane potential. Mitochondrial ROS was an upstream mediator of senescence since treatment of hCPC-1% with mitochondrial inhibitor antimycin A recapitulated

[**]**Corresponding Author:** Mark A. Sussman, PhD, SDSU Heart Institute and Department of Biology, San Diego State University, 5500 Campanile Drive, San Diego, CA 92182, Phone: (619) 594-8632, Fax: (619) 594-8635, heartman4ever@icloud.com.

[*]co-lead authors each assert majority contribution to the study so first authorship was determined alphabetically.

Kelli Korski*[1] (Conception and design, collection and assembly of data, data analysis and interpretation, manuscript writing)
Dieter Kubli*[1] (Conception and design, collection and assembly of data, data analysis and interpretation, manuscript editing)
Bingyan J. Wang[1] (Collection of data)
Farid Khalafalla[1] (Collection of data)
Megan Monsanto[1] (Collection of data)
Fareheh Firouzi[1] (Collection of data)
Oscar Echeagaray[1] (Schematic design)
Taeyong Kim[1] (Collection of data)
Robert Adamson[2] (Provision of study material)
Walter Dembitsky[2] (Provision of study material)
Åsa Gustafsson[3] (Provision of study material)
Mark Sussman[1]** (Financial support, conception and design, data analysis and interpretation, final approval of manuscript)

Disclosures

M.A.S. is CSO for CardioCreate, Inc. K.I.K. reported employment/leader opportunity with CardioCreate, Inc. All of the other authors reported no conflicts.

mitochondrial dysfunction and senescence observed in hCPC-21%. NAD^+/NADH ratio and autophagic flux, key factors for mitochondrial function, were higher in hCPC-1%, but hCPC-21% were highly dependent on BNIP3/NIX-mediated mitophagy to maintain mitochondrial function. Collectively, results demonstrate that supraphysiological oxygen tension during *in vitro* expansion initiates a downward spiral of oxidative stress, mitochondrial dysfunction, and cellular energy imbalance culminating in early proliferation arrest of hCPCs. Senescence is inhibited by preventing ROS through hypoxic culture of hCPCs.

Graphical Abstract

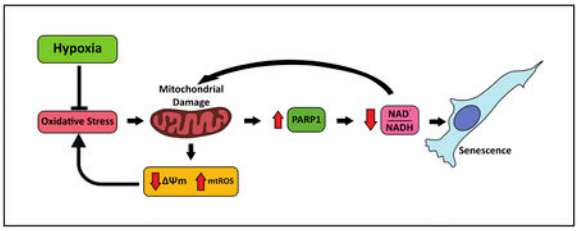

Keywords

heart; stem cells; mitochondria; ROS; autophagy; human

Introduction

Heart failure (HF) remains an intractable condition despite significant improvements in treatment of ischemic heart disease [1]. Inherently poor cardiac reparative capacity is a primary obstacle in recovering myocardial function in HF patients. One potential source to mediate reparative processes are resident c-Kit^+ cardiac progenitor cells (hCPCs) that exert modest beneficial effects in preclinical and clinical studies [2, 3]. Limited engraftment and survival of CPCs following intramyocardial delivery remains problematic, prompting repeated injections to augment efficacy and highlighting the need to improve CPC persistence [4–7]. hCPCs isolated from HF patients have endured pathological conditions that adversely affect their function and predispose them to senescence or cell death [8], rendering them biologically impaired for mediating reparative processes that are compromised as a consequence of senescence [9, 10].

Adult stem and progenitor cells are protected from environmental damage and exhaustion *in vivo* within stem cell niches [11]. Hypoxia is characteristic of stem cell niches and acts as an important environmental factor for protecting cells from metabolically acquired damage [12–14]. The cardiac CPC niche is hypoxic (~1% O_2), indicating low oxygen tension is potentially beneficial for CPC biology [15, 16]. Conventional CPC isolation and expansion is performed under normal atmospheric oxygen tension (i.e. physiological hyperoxia) of 21% O_2. Supraphysiological oxygen tension has been implicated in senescence of other cell types [17] and is likely to be a primary driving factor leading to premature senescence of cultured hCPCs. Permanent hypoxic isolation and expansion of hCPCs could mitigate or even improve senescence-associated properties by lowering oxidative stress. Indeed, short term hypoxic treatments performed on mouse and hCPCs enhance proliferation and

migration *in vitro* [18–20], but understanding of how hypoxia influences hCPCs is obscured by protocol variation in oxygen tension and duration of exposure among previous studies. Therefore, this study was designed to assess the contribution of oxidative stress to early senescence of HF hCPCs, with cell isolation and expansion performed under constant hypoxia (1% O_2). Findings indicate that normoxic culture conditions promote deleterious senescence-associated functional changes for hCPCs that are blunted and in some cases improved through the use of hypoxic conditions for isolation and expansion of hCPCs.

Materials and Methods

Human Cardiac Progenitor Cell Isolation:

Left ventricular wall tissue explants were obtained from heart failure patients undergoing left ventricular assist device (LVAD) implantation. Samples were received from consenting patients with IRB approval following NIH guidelines for human subjects research. Tissue samples were placed in cardioplegic solution on ice for transportation before being divided into two roughly equal parts for simultaneous processing under normoxic (atmospheric 21% O_2) and hypoxic (1% O_2) conditions. Subsequent steps were performed simultaneously by two individuals following identical protocols under respective oxygen conditions as previously published [21]. hCPC-21% were maintained in a standard 5% CO_2 (balance air) tissue culture incubator. hCPC-1% were isolated and maintained in 1% O_2, 5% CO_2, balance N_2 (Coy O_2 Control Glove Box). For all experiments, solutions and plastics were pre-equilibrated to respective oxygen tension. Tissue explants were placed in basic buffer (11 g/L MEM Eagle, Joklik Modification, 3 mM HEPES, 1% Penicillin-Streptomycin-Glutamine, 10 mM Taurine, Insulin in 3% Acetic Acid/PBS, 1% Amphotericin B, 50 mg Gentamicin), adipose tissue was mechanically removed and remaining myocardial tissue was minced into ~1 mm^3 pieces for collagenase type II digestion at 37°C. Following collagenase digestion (1.5 to 2 hours depending on sample size) cell suspension was centrifuged at 350 × g for 5 minutes and re-suspended in hCPC growth medium composed of Ham's Nutrient Mixture F12 (HyClone #SH30026.01) supplemented with 10% ES FBS (Gibco #16141079), 1% Penicillin-Streptomycin-Glutamine (Gibco #10378016), 5 mU/mL human erythropoietin (Sigma Aldrich #E5627), 10 ng/mL human recombinant basic FGF (Biopioneer #HRP-0011), 0.2 mM L-Glutathione (Sigma #66013–256). The cell suspension was passed through 100 μm (Corning, #352360) and 40 μm (Corning, #352340) filters to eliminate debris, followed by centrifugation at 150 × g for 2 minutes to remove cardiomyocytes. Non-cardiomyocyte cells were plated in hCPC medium overnight, then subjected to magnetic-activated cell sorting (MACS) sorting using c-kit (CD117) magnetic beads (Miltenyi Biotec, catalog #130–091-332) following manufacturer's protocol to enrich for c-kit^+ hCPCs. Cells were plated and expanded in hCPC growth medium. hCPCs used in all experiments were between passages 4 – 10. Cell culture flasks with either vented (normoxia) or plug caps (hypoxia) were used to allow for microscopic assessments outside the hypoxic chamber.

Clonogenicity Assay:

hCPCs were plated at a dilution of 1 cell/well in 72-well Terasaki plates. Immediate after plating, wells were individually analyzed to exclude wells with greater or less than 1 cell.

5μL medium was added to wells every 2 days. Colonies were counted on day 17 – 22 (dependent on confluency). A colony was defined as a well with >50% confluency. Cells were fixed with 4% PFA and washed with PBS before imaging on a Leica DMI6000 live imaging microscope.

Malondialdehyde Quantification:

One million hCPCs were re-suspended in 100 μL of PBS + butylated hydroxytoluene, followed by sonication and freezing at −80°C until day of assay. OxiSelect Thiobarbituric Acid Reactive Substances (TBARS) assay kit (Cell Biolabs, Inc, catalog # STA-330) was used for quantification of malondialdehyde following manufacturer's recommended protocol. Samples were loaded onto 96-well black-wall plates (Costar, catalog # 3370) and fluorescence was measured on a BioTek plate reader. A standard curve was used to calculate malondialdehyde concentrations.

Flow Cytometry for Marker Expression:

Cells were fixed in 4% PFA for 5 minutes, followed by two washes with 1% horse serum in PBS. Permeabilization was performed with 0.1% Triton X-100 containing 0.1 M glycine for 3 minutes, followed by PBS wash. Cells were blocked with 10% horse serum for 30 minutes, and then incubated with primary antibody in 100μL of 10% horse serum for 1 hour at room temperature, protected from light. Cells were washed 3 times before secondary application for 1 hour at room temperature, protected from light. Finally, cells were washed 3 times before final resuspension in PBS + 0.5% BSA + 2mM EDTA for flow cytometry. Data were collected on a BD FACSCanto equipped with 488nm and 633nm lasers in FITC and PerCP-Cy5.5 channels using FACS Diva Software. Gating and analyses were performed using FlowJo software, by selecting single cells of similar size and granularity (FSC/SSC) and then setting gates based on isotype controls [22].

Cell Death Assay:

hCPC-1% and hCPC-21% were plated on 6-well cell culture plates (25,000 cells/well) and incubated overnight in their respective conditions. Cells were then preconditioned for 24-hours in low serum (2.5% ES FBS) Ham's F12 medium. Cells were washed with PBS and treated with 750 μM H_2O_2 (Sigma, catalog # 43410) for four hours in low serum medium in normoxia. Both hCPC-1% and hCPC-21% were subjected to H_2O_2 treatment under normoxic conditions because hypoxia dampens effects of H_2O_2 challenge. Cells were collected and stained with annexin V (AnV) (BD Pharminogen, catalog # 550475) and propidium iodide (PI) (Life Technologies, catalog # PI304MP) to assess cell viability by flow cytometry using unstained and single-stained cells for gating controls. AnV+ cells were counted as early apoptotic, AnV+PI+ cells as late apoptotic and PI+ cells as necrotic cells. Data was collected on a BD FACSCanto and analyzed by FACS Diva Software (BD Biosciences).

Mitochondrial Stress Test:

One day before assay, hCPC-1% and hCPC-21% (15,000 cells/well) were plated on 8-well Seahorse XFp Cell Culture Miniplates (Agilent Technologies) in triplicate, leaving wells #1

and #8 blank for medium-derived background deduction. Simultaneously, cell standard curves for each condition were also plated on XFp Miniplates in duplicate (10,000; 20,000; 40,000 cells/well) for data normalization. Standard curve plate was incubated for one hour before adding CyQUANT Direct DNA-labeling fluorescent reagent (Life Technologies), followed by another 1-hour incubation. CyQUANT fluorescence was measured on a SpectraMax Plus plate reader (Molecular Devices). The next day, hypoxic cells (sealed in a BD GasPak with 1% O_2) and normoxic cells were transported to UCSD (30 minutes). Cells were washed twice with assay medium containing 1 mM pyruvate, 2 mM glutamine, and 10 mM glucose in Seahorse XF Base Medium without phenol red, and then 180 μl of assay medium was added per well. Cells were incubated for 1 hour at 37°C in a non-CO_2 incubator to equilibrate oxygen concentration prior to beginning assay. Oxygen consumption rate (OCR) data were collected using a Seahorse XFp analyzer as follows: 3 baseline measurements, 3 measurements of oligomycin-dependent State 4 (1 μM oligomycin), 3 measurements of maximal uncoupled respiration (1.5 μM FCCP), and 3 measurements of minimal, non-mitochondrial respiration (0.5 μM rotenone/antimycin A). FCCP concentration was determined empirically by titration to achieve maximal uncoupled rate. Non-mitochondrial respiration was subtracted from all other data as correction. ATP production rate was calculated as Baseline OCR – Oligomycin State 4. Data were normalized to cell number by addition of CyQUANT reagent to cells immediately after assay, followed by a 1-hour incubation at 37°C in a 5% CO_2 incubator and fluorescence detection on the same SpectraMax Plus plate reader used for establishing standard curves the day prior.

Metabolic Assessments:

For ATP quantitation, 75,000 cells were plated overnight in T-25 flasks overnight. The following day, cells were trypsinized, counted, and 50,000 cells were lysed in Nucleotide Releasing Buffer (Abcam). Lysates were immediately used for ATP quantitation by bioluminescence assay (Abcam catalog #65313). For lactate production, glutamine uptake, and glutamate secretion assays, 5,000 cells were plated per well on 96-well plates overnight. The following day, media were refreshed. Samples of media (including cell-free blank wells) were collected at T = 0 hours and T = 48 hours, diluted 1:20 in PBS, and stored at −20°C. Media samples were analyzed using Lactate-Glo and Glutamine/Glutamate-Glo assays (Promega).

Mitochondrial Membrane Potential (ΔΨm):

hCPC-1% and hCPC-21% were plated in T-25 flasks (50,000 cells) in full medium. The next day, cells were washed with PBS and fresh medium was added prior to experiment. MitoProbe JC-1 Assay Kit was used (Life technologies, catalog # M34152) to measure mitochondrial membrane potential following manufacturer's protocol. JC-1 fluorescence was measured by flow cytometry (BD FACSCanto) and data were analyzed using FlowJo software. Cell populations were selected as described above, and median FITC and PE fluorescence were used to calculate a red:green ratio as an index of ΔΨm. 50 μM carbonyl cyanide m-chlorophenyl hydrazine (CCCP) was used as a control for dye responsiveness and to establish fluorescence profile of uncoupled cells.

MtDNA Assessment:

Mitochondrial DNA copy number was determined as previously described [23]. Genomic and mitochondrial DNA were isolated from normoxic and hypoxic hCPCs plated the day before (50,000 cells/T25) by NucleoSpin DNA extraction kit (Macherey-Nagel, catalog # 740952.250) following manufacturer's protocol. Total DNA was quantified by Qubit fluorometer (Thermo Fisher Scientific). Using real-time PCR, mitochondrial DNA was calculated relative to nuclear DNA as: Relative mtDNA content = $2 \times 2^{\Delta Ct}$, where ΔCt = (nucDNA Ct – mtDNA Ct). Primers are listed in Supplemental Table 1. PCR cycle protocol used was: 94°C for 2 minutes; 40 cycles of: 94°C for 30 sec; 62°C annealing temperature for 30 sec; and 72°C for 1 minute; 5 minutes at 72°C.

Immunoblot Analysis:

Detailed methods available in Online Supplement. Antibodies and concentrations are listed in Supplemental Table 2.

Autophagic Flux and Mitophagy Assessments:

For measurements of autophagic flux 150,000 Human hCPCs were plated on T-25 flasks overnight before treatment with 50 nM Bafilomycin A1 (Millipore, catalog # 508409) or DMSO vehicle control for 6 hours. Cells lysates were prepared for immunoblot analysis. Alternatively, cells were treated for 24 hours with 50 nM Bafilomycin A1 prior to assessing $\Delta\Psi m$ by JC-1 staining and flow cytometry as described above.

Mitophagy Confocal Imaging Analysis:

Cells were plated on 2-well Permanox chamber slides (Nunc Lab-Tek) overnight, and treated with 50 nM Bafilomycin A1 for 6 hours before being fixed with 4% PFA, washed with PBS, and permeabilized with 0.2% Triton X-100 for 5 minutes at room temperature. Cells were washed again with PBS followed by 0.1 M glycine wash for 10 minutes. Cells were blocked with 5% normal donkey serum in PBS for 30 minutes, and then incubated with antibodies directed against LC3 and MTCO1 (Supplemental Table 2) in 5% normal donkey serum overnight. The following day, cells were washed, incubated with secondary antibodies for one hour (donkey anti-rabbit AlexaFluor 488 and donkey anti-mouse AlexaFluor555), washed again, stained with Hoechst 33342 (Thermo) to label nuclei, and finally coverslipped with VectaShield (Vector Labs). Images were captured on a Leica SP8 confocal microscope using consistent laser power, pinhole, and settings. Colocalization analysis was performed using ImageJ software using ComDet plugin. For each experiment, 20 cells were quantified per condition, and mean of three independent experiments were calculated.

Mitochondrial Superoxide Quantification:

hCPC-1% and hCPC-21% from matching passages were plated on 6-well plates (25,000 cells/well) overnight. The following day, cells were washed, and 2 mL of fresh medium was added. Cells were incubated with 5 μM MitoSOX Red (Life Technologies, catalog # M36008) for 30 minutes before being lifted, pelleted and washed twice in 0.5% BSA in PBS, prior to analysis on a BD Canto flow cytometer. Data were analyzed on BD FACSDiva Software.

Single-cell RNA library preparation and sequencing:

Human CPCs cultured at 21% O_2 were suspended and washed with PBS, centrifuged and resuspended in 0.04% non-acetylated bovine serum albumin to an approximate cell concentration of 200 cells/μl. Cell suspensions were loaded on a Chromium™ Controller (10X Genomics) to generate single-cell Gel Bead-In-EMulsions (GEMs). Single-cell RNA-Seq libraries were prepared using Chromium™ Single Cell 3' Library & Gel Bead Kit v2 (10X Genomics). GEM-reverse transcription (RT) was performed in a C1000 Touch Thermal cycler with TempAssure PCR 8-tube strip (USA Scientific): 55 °C for 2 h, 85 °C for 5 min; held at 4 °C. After RT, GEMs were broken, and single-strand cDNA was cleaned up with DynaBeads MyOne Silane Beads (Thermo Fisher Scientific) and SPRIselect Reagent Kit (0.6X SPRI; Beckman Coulter). cDNA was amplified by C1000 Touch Thermal cycler with TempAssure PCR 8-tube strips: 98 °C for 3 min; cycled 14X: 98 °C for 15 sec, 67 °C for 20 sec, and 72 °C for 1 min; 72 °C for 1 min; held at 4 °C. Amplified cDNA product was cleaned up with SPRIselect Reagent Kit (0.6X SPRI). Indexed sequencing libraries were constructed using Chromium™ Single Cell 3' Library & Gel Bead Kit v2, following these steps: (1) end repair and A-tailing; (2) adapter ligation; (3) post-ligation cleanup with SPRIselect; (4) sample index PCR and cleanup. Quality control for each library was performed by Bioanalyzer (average library size: 450–490 bp). Sequencing libraries were quantified by quantitative PCR (KAPA Biosystems Library Quantification Kit for Illumina platforms P/N KK4824) and Qubit 3.0 using dsDNA HS Assay Kit (Thermo Fisher Scientific) prior to loading on an Illumina NextSeq500 using the following read length: 98 bp Read1, 8 bp i7 Index, and 26 bp Read2.

Analysis of single-cell RNA-seq data:

Raw data was demultiplexed, aligned to reference genome, filtered, and counted using Cell Ranger pipeline (10X Genomics; version 1.3.1). Sequencing reads were aligned to human genome GRCh38. Cells with less than 1,000 genes or more than 10% mitochondrial gene UMI count were filtered out, and genes detected in less than three cells were filtered out. Principal Component Analysis dimensionality reduction was performed by CellRanger pipeline. Significant principal components were used to generate a t-stochastic neighbor embedding (t-SNE) projection [24, 25] and unsupervised clustering [26]. Expression assessment of mitophagy associated genes (*PARK2, BNIP3, BNIP3L* and *FUNDC1*) was performed and visualized through Loupe Cell Browser 2.0.0.

Statistical Analysis:

Data are presented as mean ± standard deviation (SD). For comparisons of two groups, Student's t-test was used to determine significance. For comparisons of multiple groups, one-way ANOVA was performed followed by Tukey-Kramer post hoc test. Statistics were performed using GraphPad Prism software.

Results

Self-Renewal Is Increased and Senescence Decreased by Long-term Hypoxia of hCPCs.

hCPCs were isolated from three patients undergoing LVAD implantation. In each isolation, the obtained tissue explant was divided in half and processed in hypoxia (1% O_2, "hCPC-1%") or normoxia (ambient air ~21% O_2, "hCPC-21%") to isolate and expand c-Kit $^+$ hCPCs. hCPC-1% were never exposed to ambient oxygen tension unless necessary for a specific experiment. All established lines (h106, h111 and h112) were from male patients (ages 62, 61, 42 respectively) with a history of hypertension and smoking prior to developing HF (Supplemental Table 3). Normoxic and hypoxic cells from all three lines were positive for c-KIT, CD34, and CD105, and showed variable expression of CD166 by flow cytometry (Supplemental Figures S1 & S2). Marker expression resembles profiles of CPCs previously characterized by our lab and others [21, 27], and suggest a relatively homogeneous population of cultured CPCs, in agreement with recently published results demonstrating transcriptomic convergence following cell isolation and culture [28].

Clone formation is a primary characteristic of stem cells and is a readout for self-renewal potential. Self-renewal was measured by quantifying clone formation from single cells in hCPC-1% and hCPC-21%. Although all tested lines formed colonies, lines h112 (11% ± 2 $p<0.001$) and h111 (21% ± 3 $p<0.001$) formed significantly more colonies in hypoxia versus normoxia (Figure 1A, 1B & Supplemental Figure S3). Line h106 demonstrated high self-renewal under normoxia and thus did not significantly improve under hypoxia (3% ± 3). Line h111 showed the largest improvement in self-renewal under hypoxia and was therefore unlikely to be representative of an average phenotype. Line h112 was selected for subsequent experiments based on its intermediate improvement in self-renewal under hypoxia. hCPC-21% from line h112 were large and flat, characteristic of senescent cells, while hCPC-1% maintained a small, spindle-shaped morphology (Figure 1A). Senescence-associated β-Gal positivity was used as a marker of cellular senescence. hCPC-1% exhibited ~70% fewer SA-β-Gal+ cells than hCPC-21% (Figure 1C, 1D), suggesting hypoxia delays hCPC senescence and supports self-renewal. Morphological assessment demonstrated hCPC-1% maintained smaller area within passages 4–10 (Figure 1E, 1F).

Oxidative Stress Is Attenuated and Survival Enhanced in Hypoxic hCPCs.

Oxidative stress is a major contributing factor in cell senescence [29, 30]. Markers of oxidative stress were investigated in hCPC-1% and hCPC-21%. Malondialdehyde (MDA) content was measured as an indicator of lipid peroxidation. MDA concentrations were 82% lower in hCPC-1% compared to hCPC-21% (0.3 ± 0.03 μM vs. 1.8 ± 0.3 μM per 1×10^6 cells, respectively; Figure 2A). Oxidative stress can also cause DNA damage, thereby promoting senescence [31]. To assess DNA damage, nuclear γH2AX foci were quantified as a marker of double stranded DNA break repair. The number of γH2AX foci per nucleus was significantly lower in hCPC-1% (Figure 2B, 2C) demonstrating mitigation of DNA damage. hCPC-1% were substantially more resistant to cell death and retained 77% healthy cells versus only ~60% healthy cells in hCPC-21% after 4 hours of H_2O_2 treatment (Figure 2D, Supplemental Figure S4). Dying cells were divided into groups of early apoptosis, late apoptosis and necrosis based on Annexin V and PI staining. hCPC-1% showed significantly

fewer cells in late apoptosis and necrosis compared to hCPC-21% (Figure 2E). These results demonstrate that hypoxia not only protected hCPCs against environmentally acquired oxidative damage, but also improved resistance to oxidative stress-induced cell death.

Mitochondrial Function Is Preserved by hCPC Hypoxic Culture.

Mitochondrial respiration is a primary source of cellular ROS generation with cells in higher oxygen tension predicted to have higher respiration rate[32]. hCPC oxygen consumption rate (OCR) was measured to assess relationships between OCR and oxidative stress marker levels. Surprisingly, basal and maximal uncoupled OCR, as well as oxygen consumption-coupled ATP production, were significantly higher in hCPC-1% compared to hCPC-21% (Figure 3A–3D). Due to technical limitations of Seahorse assay, OCR was measured under normoxic conditions for all cells. Therefore, mitochondrial membrane potential ($\Delta\Psi m$) was assessed under hypoxia to corroborate findings that hypoxic CPCs had higher mitochondrial function. hCPC-1% had significantly higher $\Delta\Psi m$ than hCPC-21% (Figure 3E, Supplemental Figure S5), confirming elevated mitochondrial function in hCPC-1%. Further, hCPC-1% had significantly higher cellular ATP content, but lower lactate production and glutamate secretion rates (Supplemental Figure S6), indicating lower glycolysis and glutaminolysis respectively. Contrary to expectations, hCPC-1% were therefore more reliant oxidative metabolism and less reliant on glycolytic and glutaminolytic energy production pathways than hCPC-21%.

Mitochondrial function, ATP production, and prevention of cellular senescence are dependent on maintaining high cellular NAD^+/NADH ratio. Activation of poly(ADP)ribose polymerase-1 (PARP-1) in response to DNA damage (shown in Figure 2B & 2C) is known to deplete cellular NAD^+ and promote senescence [33]. NAD^+/NADH ratio was 2.3-fold higher in hCPC-1% than in hCPC-21% (Figure 3F), while PARP-1 expression was 3.6-fold higher in hCPC-21% (Figure 3G, 3H). Maintenance of NAD^+ levels due to decreased PARP-1 expression could therefore contribute to improved mitochondrial function and delayed senescence in hCPC-1%.

Mitochondrial Content Is Decreased by Hypoxic hCPC Culture.

Mitochondrial quantity was assessed to further investigate the reason for elevated OCR in hypoxic cells. In contrast to their higher OCR, hCPC-1% unexpectedly had 42% lower mitochondrial DNA content than hCPC-21%, indicative of lower mitochondrial volume density (Figure 4A). Protein expression levels of subunits from ETC complex I, complex IV and ATP synthase were also significantly reduced in hCPC-1%, indicating lower respiratory chain protein abundance (Figure 4B-4G). Thus, despite having higher mitochondrial respiration rates, hCPC-1% had lower mitochondrial content than hCPC-21%. TEM also revealed that hCPC-1% mitochondria were more compact and had higher cristae density than hCPC-1% mitochondria (Figure 4H). Together, these results suggest that hypoxic CPCs maintain higher quality mitochondria, producing higher OCR per mitochondrial volume density, and suggests that mitochondrial dysfunction underlies oxidative stress observed in hCPC-21%.

Senescence Is Accelerated by Mitochondrial ROS Induction in Hypoxic hCPCs.

Improved mitochondrial function and decreased senescence in hCPC-1% implicates mitochondrial-derived ROS as a factor in hCPC senescence. Elevated superoxide generation in hCPC-21% was confirmed by flow cytometry showing nearly two-fold higher MitoSOX Red fluorescence intensity in hCPC-21% versus hCPC-1% (Figure 5A). Mitochondrial ROS was subsequently artificially increased while maintaining hypoxic conditions by inhibition of complex III with 100 μM antimycin A (AMA) for 9 days in hCPC-1% (Figure 5B). $\Delta\Psi m$ decreased by 57% in hCPC-1% after AMA treatment (Figure 5C), but AMA had no effect on cell viability (Figure 5D, 5E). However, a 220% increase in SA-β-gal+ positive cells was observed in hCPC-1% treated with AMA, suggesting mitochondrial ROS can directly drive hCPC senescence (Figure 5C, 5D). Elevated mitochondrial ROS caused by mitochondrial dysfunction therefore results in senescence of hCPCs.

BNIP3/NIX-Mediated Mitophagy Supports Mitochondrial Function In Normoxic hCPCs.

Removal of dysfunctional mitochondria occurs through mitophagy. Impaired mitophagy may therefore contribute to decreased mitochondrial function. First, general autophagy was assessed to determine if hypoxia impacted cellular housekeeping functions that may influence cell senescence. hCPC-1% had significantly lower basal levels of both cytosolic and autophagosome-linked autophagy-related protein LC3 (LC3I and LC3II, respectively, Figure 6A–6C). However, when lysosomal degradation was inhibited with Bafilomycin A1, hCPC-1% showed a larger induction of LC3II (compared to baseline), indicating increased autophagic flux compared to hCPC-21% (Figure 6D, 6E). To assess mitophagy, autophagosomes and mitochondria labeled with antibodies for LC3 and complex IV subunit 1 (MTCO1) were quantified by confocal microscopy (Supplemental Figure S7A). Both hCPC-21% and hCPC-1% significantly increased autophagosome quantity per cell after 6 hours of Bafilomycin A1 treatment (Supplemental Figure S7B). hCPC-1% also trended toward lower colocalization percentage between autophagosomes and mitochondria under both control and Bafilomycin A1-treated conditions compared to hCPC-21% (Supplemental Figure S7C). Cells were then treated with Bafilomycin A1 for 24 hours and $\Delta\Psi m$ was measured by JC-1 staining and flow cytometry to determine effects of lysosome inhibition on mitochondrial function. hCPC-21% showed a significant decline in $\Delta\Psi m$ after treatment while hCPC-1% showed minimal effects on $\Delta\Psi m$ (Figure 6F, 6G, and Supplemental Figure S8), demonstrating that hCPC-21% have a greater reliance on mitophagy to maintain $\Delta\Psi m$. hCPC-1% require less mitophagy to maintain $\Delta\Psi m$ likely due to lower ROS generation.

Mitophagy can occur through Parkin-dependent or Parkin-independent pathways. Parkin-mediated mitophagy follows total loss of $\Delta\Psi m$ [34, 35], while mitophagy through direct receptors such as BNIP3 and NIX occurs in dysfunctional mitochondria retaining low $\Delta\Psi m$ [36, 37]. Parkin transcripts (*PARK2*) were only very rarely detected in hCPC-21% by single cell RNA sequencing, while transcripts of BNIP3 and NIX (*BNIP3* and *BNIP3L*, respectively) were detected in the majority of cells (Supplemental Figure S9). *FUNDC1*, another mitophagy receptor, was expressed in about 30% of hCPCs. While Parkin-mediated mitophagy is therefore unlikely to be the primary mechanism for mitochondrial quality control in hCPCs, BNIP3, NIX, and to a lesser extent FUNDC1 are likely predominant mitophagy pathways. BNIP3 and NIX protein levels were found to be significantly lower in

hCPC-1% (Figure 6H–6J), reflecting a lower requirement for mitophagy to remove damaged mitochondria in these cells compared to hCPC-21%.

Discussion

Early replicative senescence and susceptibility of hCPCs to cell death were attributed to oxidative stress caused by culture in supraphysiological oxygen conditions. This study shows that self-renewal and survival of hCPCs can be significantly improved by permanent hypoxic expansion through preservation of high mitochondrial function. Therefore, isolation and expansion of hCPCs in low oxygen tension is a viable approach to potentiate hCPC mitochondrial function, minimize ROS generation, and mitigate cellular senescence.

Short term hypoxic preconditioning increases proliferation, reduced senescence, and resistance to cell death in mouse and human CPCs [19, 20]. However, the potential of hypoxia to impart beneficial effects to cells isolated from pathologically diseased tissue through permanent hypoxic culture had not previously been performed in HF patient hCPCs. Instead of observing persistence of cellular damage from diseased tissue carrying over to cells *in vitro*, hypoxia was found to bolster mitochondrial function and suppress mitochondrial ROS. Mesenchymal stromal cells from human patients with atherosclerosis also exhibit increased ROS and mitochondrial dysfunction compared to cells from non-atherosclerotic patients [38, 39]. Three hCPC-1% lines examined here exhibited improved clonogenicity and lower senescence compared to hCPC-21%, albeit to varying degrees (Figure 1). Differences in responsiveness to hypoxia are likely due to human sample variations and specific disease etiologies [40]. Hypoxic culture also improved resistance to oxidative insults (Figure 2). These results agree with previous studies that demonstrate a positive association between reduced oxygen tension and suppressed senescence [41], and also encouragingly suggest that CPCs isolated from diseased hearts are not predestined to be frangible, but can be fortified by appropriate *in vitro* conditions.

Mitochondrial dysfunction has recently been implicated in driving a unique senescent state with a characteristic secretory phenotype in cells that undergo mitochondrial dysfunction-associated senescence (MiDAS). Chronic activation of energy-producing pathways caused by low cellular NAD^+/NADH ratio eventually lead to p53 activation and cell cycle exit. The senescent phenotype observed in hCPC-21% bears a striking resemblance to MiDAS, with a decline in NAD^+/NADH ratio and impaired mitochondrial function [42]. A major distinction between the studies is that Wiley et al. used chemical respiratory chain inhibition to drive MiDAS, whereas hCPCs cultured in normoxia appear to spontaneously develop mitochondrial dysfunction. It remains unknown whether spontaneous impaired mitochondrial dysfunction-induced senescence observed in hCPC-21% is unique to progenitor cells or common to all cells undergoing replicative senescence *in vitro*.

NAD^+/NADH ratio is an important cellular index influencing mitochondrial function [42]. NAD^+/NADH ratio was found to be significantly lower in hCPC-21% than in hCPC-1%, likely through PARP-1 activation (Figure 3). PARP-1 consumes NAD^+ to recruit repair enzymes to single-stranded DNA breaks [43, 44]. PARP-1 activation in response to simulated hypoxia-reperfusion injury can deplete NAD^+ and ATP, as well as blunt

mitochondrial function [45]. Chronic activation of PARP-1 exacerbates cellular senescence progression [46]. hCPC-1% exhibited less DNA damage than hCPC-21%, suggesting an increased requirement for DNA damage response (DDR) in hCPC-21% leading to NAD^+ exhaustion. Low levels of NAD^+ have been associated with aging in several tissues [47–49]. NAD^+ repletion by administration of NAD^+ precursors improves mitochondrial function and blunts senescence in aged mice [50]. Future studies will determine whether NAD^+ repletion can reverse the senescent phenotype and restore mitochondrial function of hCPC-21%.

Dysfunctional mitochondria generate cellular ROS that can perpetuate further mitochondrial damage [32, 51], while maintenance of high mitochondrial function is imperative to avoid MiDAS. Oxidative stress can also lead to impaired lysosomal degradation, thereby reducing autophagic flux, increasing mitochondrial mass, and initiating senescence [52–54]. The observations that hCPC-21% have higher mitochondrial mass, lower autophagic flux and increased reliance on mitophagy to maintain mitochondrial function may therefore represent both a root cause of mitochondrial dysfunction and senescence, and a consequence of oxidative stress. Notably, mitophagy in hCPCs appears to primarily occur through mitophagy receptors BNIP3 and NIX that link mitochondria to LC3-decorated autophagosomes, rather than through PINK1 and PARKIN. BNIP3 and NIX-mediated mitophagy may be activated in damaged but still-functional mitochondria [36], while PARKIN is upregulated and activated in response to catastrophic mitochondrial depolarization and injury [34, 55]. Experiments using respiratory chain inhibition to induce ROS production in hCPC-1% implicate mitochondrial dysfunction as directly causative of hCPC senescence (Figure 5). The net result is a feed-forward cycle of oxidative damage and dysfunctional mitochondria, further requiring mitophagy and promoting hCPC senescence (Figure 7).

Similarly to hCPCs, hypoxia benefits human mesenchymal stem cells (hMSCs) by supporting self-renewal and mitigating senescence [56, 57]. Combinatorial delivery of human MSCs (hMSC) and hCPCs into infarcted swine hearts shows a two-fold reduction in scar size and significant improvement in LV function over either cell type alone [58, 59]. Concurrent isolation and expansion of hMSCs and hCPCs from HF patients [21] under permanent hypoxia prior to combinatorial delivery to restore functional competency could further enhance outcomes of cell-based therapy. Given that current transplantation strategies yield extremely short persistence of engrafted cells, future studies will explore whether hypoxic expansion of hCPCs impacts persistence and function post engraftment.

Conclusions

This study introduces a novel approach for augmenting hCPC self-renewal and survival by maintaining mitochondrial function and blunting senescence. The ability of hypoxia to delay hCPC senescence hinges on prevention of mitochondrial dysfunction and dampened ROS production. Mitochondrial ROS play a causative role in hCPC senescence by promoting mitochondrial dysfunction and oxidative stress, additionally sensitizing hCPCs to cell death. This important finding opens many doors for future strategies to target augmented hCPC mitochondrial quality by enhancing mitophagy or reestablishing cellular bioenergetics, NAD^+/NADH, and redox status. Permanent hypoxic expansion of HF patient hCPCs is a powerful

method for safely improving cell quality by reducing hCPC sensitivity to oxidative stress and enhancing *in vitro* expansion potential.

Supplementary Material

Refer to Web version on PubMed Central for supplementary material.

Acknowledgements

We thank Dr. Ingrid Niesman and the SDSU Electron Microscope Imaging Facility for sample processing, specimen preparation and general assistance.

Funding

M.A. Sussman is supported by NIH grants: R01HL117163, R01HL122525, R01HL135661, R37HL091102, R41HL137602, P01HL085577 as well as a grant from the Fondation Leducq. D.A. Kubli is funded by NIH fellowship F32HL136064.

References

1. Benjamin EJ, Blaha MJ, Chiuve SE, et al. Heart Disease and Stroke Statistics-2017 Update: A Report From the American Heart Association. CIRCULATION 2017;135(10):e146–e603. [PubMed: 28122885]
2. Chugh AR, Beache GM, Loughran JH, et al. Administration of cardiac stem cells in patients with ischemic cardiomyopathy: the SCIPIO trial: surgical aspects and interim analysis of myocardial function and viability by magnetic resonance. CIRCULATION 2012;126(11 Suppl 1):S54–64. [PubMed: 22965994]
3. Kulandavelu S, Karantalis V, Fritsch J, et al. Pim1 Kinase Overexpression Enhances ckit+ Cardiac Stem Cell Cardiac Repair Following Myocardial Infarction in Swine. J. AM. COLL. CARDIOL 2016;68(22):2454–2464. [PubMed: 27908351]
4. Garbern JC, Lee RT. Cardiac stem cell therapy and the promise of heart regeneration. CELL STEM CELL 2013;12(6):689–698. [PubMed: 23746978]
5. Guo Y, Wysoczynski M, Nong Y, et al. Repeated doses of cardiac mesenchymal cells are therapeutically superior to a single dose in mice with old myocardial infarction. BASIC RES. CARDIOL 2017;112(2):18. [PubMed: 28210871]
6. Tang X-L, Nakamura S, Li Q, et al. Repeated Administrations of Cardiac Progenitor Cells Are Superior to a Single Administration of an Equivalent Cumulative Dose. J AM HEART ASSOC 2018;7(4).
7. Tokita Y, Tang X-L, Li Q, et al. Repeated Administrations of Cardiac Progenitor Cells Are Markedly More Effective Than a Single Administration: A New Paradigm in Cell Therapy. CIRC. RES 2016;119(5):635–651. [PubMed: 27364016]
8. Cesselli D, Beltrami AP, D'Aurizio F, et al. Effects of age and heart failure on human cardiac stem cell function. AM. J. PATHOL 2011;179(1):349–366. [PubMed: 21703415]
9. Jurk D, Wilson C, Passos JF, et al. Chronic inflammation induces telomere dysfunction and accelerates ageing in mice. NAT COMMUN 2014;2(1):4172. [PubMed: 24960204]
10. Baker DJ, Wijshake T, Tchkonia T, et al. Clearance of p16Ink4a-positive senescent cells delays ageing-associated disorders. NATURE 2011;479(7372):232–236. [PubMed: 22048312]
11. Scadden DT. The stem-cell niche as an entity of action. NATURE 2006;441(7097):1075–1079. [PubMed: 16810242]
12. Morikawa T, Takubo K. Hypoxia regulates the hematopoietic stem cell niche. PFLUGERS ARCH 2015;468(1):13–22. [PubMed: 26490456]
13. Suda T, Takubo K, Semenza GL. Metabolic regulation of hematopoietic stem cells in the hypoxic niche. CELL STEM CELL 2011;9(4):298–310. [PubMed: 21982230]

14. Ito K, Suda T. Metabolic requirements for the maintenance of self-renewing stem cells. NAT. REV. MOL. CELL BIOL 2014;15(4):243–256. [PubMed: 24651542]
15. Sanada F, Kim J, Czarna A, et al. c-Kit-positive cardiac stem cells nested in hypoxic niches are activated by stem cell factor reversing the aging myopathy. CIRC. RES 2014;114(1):41–55. [PubMed: 24170267]
16. Leri A, Rota M, Hosoda T, et al. Cardiac stem cell niches. STEM CELL RES 2014;13(3 Pt B): 631–646. [PubMed: 25267073]
17. Leontieva OV, Natarajan V, Demidenko ZN, et al. Hypoxia suppresses conversion from proliferative arrest to cellular senescence. PROC. NATL. ACAD. SCI. U.S.A 2012;109(33): 13314–13318. [PubMed: 22847439]
18. Bellio MA, Rodrigues CO, Landin AM, et al. Physiological and hypoxic oxygen concentration differentially regulates human c-Kit+ cardiac stem cell proliferation and migration. AM. J. PHYSIOL. HEART CIRC. PHYSIOL 2016;311(6):H1509–H1519. [PubMed: 27694215]
19. Tang YL, Zhu W, Cheng M, et al. Hypoxic preconditioning enhances the benefit of cardiac progenitor cell therapy for treatment of myocardial infarction by inducing CXCR4 expression. CIRC. RES 2009;104(10):1209–1216. [PubMed: 19407239]
20. Xu R, Sun Y, Chen Z, et al. Hypoxic Preconditioning Inhibits Hypoxia-induced Apoptosis of Cardiac Progenitor Cells via the PI3K/Akt-DNMT1-p53 Pathway. SCI REP 2016;6(1):30922. [PubMed: 27488808]
21. Monsanto MM, White KS, Kim T, et al. Concurrent Isolation of 3 Distinct Cardiac Stem Cell Populations From a Single Human Heart Biopsy. CIRC. RES 2017;121(2):113–124. [PubMed: 28446444]
22. Alvarez DF, Helm K, DeGregori J, et al. Publishing flow cytometry data. AM. J. PHYSIOL. LUNG CELL MOL. PHYSIOL 2010;298(2):L127–30. [PubMed: 19915158]
23. Rooney JP, Ryde IT, Sanders LH, et al. PCR based determination of mitochondrial DNA copy number in multiple species. METHODS MOL. BIOL 2015;1241:23–38. [PubMed: 25308485]
24. van der Maaten L Accelerating t-SNE using Tree-Based Algorithms. JOURNAL OF MACHINE LEARNING RESEARCH 2014;15:3221–3245.
25. Maaten LVD, Hinton G. Visualizing Data using t-SNE. JOURNAL OF MACHINE LEARNING RESEARCH 2008;9(Nov):2579–2605.
26. Macosko EZ, Basu A, Satija R, et al. Highly Parallel Genome-wide Expression Profiling of Individual Cells Using Nanoliter Droplets. CELL 2015;161(5):1202–1214. [PubMed: 26000488]
27. Le T, Chong J. Cardiac progenitor cells for heart repair. CELL DEATH DISCOV 2016;2:16052. [PubMed: 27551540]
28. Kim T, Echeagaray OH, Wang BJ, et al. In situ transcriptome characteristics are lost following culture adaptation of adult cardiac stem cells. SCI REP 2018;8(1):12060. [PubMed: 30104715]
29. Gambino V, De Michele G, Venezia O, et al. Oxidative stress activates a specific p53 transcriptional response that regulates cellular senescence and aging. AGING CELL 2013;12(3): 435–445. [PubMed: 23448364]
30. Kumar D, Rizvi SI. Markers of oxidative stress in senescent erythrocytes obtained from young and old age rats. REJUVENATION RES 2014;17(5):446–452. [PubMed: 25065263]
31. Dizdaroglu M, Jaruga P. Mechanisms of free radical-induced damage to DNA. FREE RADIC. RES 2012;46(4):382–419. [PubMed: 22276778]
32. Murphy MP. How mitochondria produce reactive oxygen species. BIOCHEM. J 2009;417(1):1–13. [PubMed: 19061483]
33. Alano CC, Garnier P, Ying W, et al. NAD+ depletion is necessary and sufficient for poly(ADP-ribose) polymerase-1-mediated neuronal death. J. NEUROSCI 2010;30(8):2967–2978. [PubMed: 20181594]
34. Narendra D, Tanaka A, Suen D-F, et al. Parkin is recruited selectively to impaired mitochondria and promotes their autophagy. J. CELL BIOL 2008;183(5):795–803. [PubMed: 19029340]
35. Narendra DP, Jin SM, Tanaka A, et al. PINK1 is selectively stabilized on impaired mitochondria to activate Parkin. Green DR, ed. PLOS BIOL 2010;8(1):e1000298. [PubMed: 20126261]

36. Zhang H, Bosch-Marce M, Shimoda LA, et al. Mitochondrial autophagy is an HIF-1-dependent adaptive metabolic response to hypoxia. J. BIOL. CHEM 2008;283(16):10892–10903. [PubMed: 18281291]
37. Zhu Y, Massen S, Terenzio M, et al. Modulation of serines 17 and 24 in the LC3-interacting region of Bnip3 determines pro-survival mitophagy versus apoptosis. J. BIOL. CHEM 2013;288(2): 1099–1113. [PubMed: 23209295]
38. Kizilay Mancini O, Lora M, Cuillerier A, et al. Mitochondrial Oxidative Stress Reduces the Immunopotency of Mesenchymal Stromal Cells in Adults With Coronary Artery Disease. CIRC. RES 2018;122(2):255–266. [PubMed: 29113965]
39. Kizilay Mancini O, Lora M, Shum-Tim D, et al. A Proinflammatory Secretome Mediates the Impaired Immunopotency of Human Mesenchymal Stromal Cells in Elderly Patients with Atherosclerosis. STEM CELLS TRANSL MED 2017;6(4):1132–1140. [PubMed: 28194905]
40. Mayfield AE, Fitzpatrick ME, Latham N, et al. The impact of patient co-morbidities on the regenerative capacity of cardiac explant-derived stem cells. STEM CELL RES THER 2016;7(1):S54.
41. Parrinello S, Samper E, Krtolica A, et al. Oxygen sensitivity severely limits the replicative lifespan of murine fibroblasts. NAT. CELL BIOL 2003;5(8):741–747. [PubMed: 12855956]
42. Wiley CD, Velarde MC, Lecot P, et al. Mitochondrial Dysfunction Induces Senescence with a Distinct Secretory Phenotype. CELL METABOLISM 2016;23(2):303–314. [PubMed: 26686024]
43. Sims JL, Berger SJ, Berger NA. Effects of nicotinamide on NAD and poly(ADP-ribose) metabolism in DNA-damaged human lymphocytes. J SUPRAMOL STRUCT CELL BIOCHEM 1981;16(3):281–288. [PubMed: 6458707]
44. Mendelsohn AR, Larrick JW. The NAD+/PARP1/SIRT1 Axis in Aging. REJUVENATION RES 2017;20(3):244–247. [PubMed: 28537485]
45. Fiorillo C, Ponziani V, Giannini L, et al. Protective effects of the PARP-1 inhibitor PJ34 in hypoxic-reoxygenated cardiomyoblasts. CELL. MOL. LIFE SCI 2006;63(24):3061–3071. [PubMed: 17131054]
46. Efimova EV, Mauceri HJ, Golden DW, et al. Poly(ADP-ribose) polymerase inhibitor induces accelerated senescence in irradiated breast cancer cells and tumors. CANCER RES 2010;70(15): 6277–6282. [PubMed: 20610628]
47. Braidy N, Guillemin GJ, Mansour H, et al. Age related changes in NAD+ metabolism oxidative stress and Sirt1 activity in wistar rats. Xu A, ed. PLOS ONE 2011;6(4):e19194. [PubMed: 21541336]
48. Gomes AP, Price NL, Ling AJY, et al. Declining NAD(+) induces a pseudohypoxic state disrupting nuclear-mitochondrial communication during aging. CELL 2013;155(7):1624–1638. [PubMed: 24360282]
49. Stein LR, Imai S-I. Specific ablation of Nampt in adult neural stem cells recapitulates their functional defects during aging. EMBO J 2014;33(12):1321–1340. [PubMed: 24811750]
50. Zhang H, Ryu D, Wu Y, et al. NAD^+ repletion improves mitochondrial and stem cell function and enhances life span in mice. SCIENCE 2016;352(6292):1436–1443. [PubMed: 27127236]
51. Balaban RS, Nemoto S, Finkel T. Mitochondria, oxidants, and aging. CELL 2005;120(4):483–495. [PubMed: 15734681]
52. Tai H, Wang Z, Gong H, et al. Autophagy impairment with lysosomal and mitochondrial dysfunction is an important characteristic of oxidative stress-induced senescence. AUTOPHAGY 2017;13(1):99–113. [PubMed: 27791464]
53. Korolchuk VI, Miwa S, Carroll B, et al. Mitochondria in Cell Senescence: Is Mitophagy the Weakest Link? EBIOMEDICINE 2017;21:7–13. [PubMed: 28330601]
54. Luo C, Li Y, Wang H, et al. Mitochondrial accumulation under oxidative stress is due to defects in autophagy. J. CELL. BIOCHEM 2013;114(1):212–219. [PubMed: 22903604]
55. Kubli DA, Zhang X, Lee Y, et al. Parkin protein deficiency exacerbates cardiac injury and reduces survival following myocardial infarction. J. BIOL. CHEM 2013;288(2):915–926. [PubMed: 23152496]

56. Fehrer C, Brunauer R, Laschober G, et al. Reduced oxygen tension attenuates differentiation capacity of human mesenchymal stem cells and prolongs their lifespan. AGING CELL 2007;6(6): 745–757. [PubMed: 17925003]

57. Basciano L, Nemos C, Foliguet B, et al. Long term culture of mesenchymal stem cells in hypoxia promotes a genetic program maintaining their undifferentiated and multipotent status. BMC CELL BIOL 2011;12(1):12. [PubMed: 21450070]

58. Williams AR, Hatzistergos KE, Addicott B, et al. Enhanced effect of combining human cardiac stem cells and bone marrow mesenchymal stem cells to reduce infarct size and to restore cardiac function after myocardial infarction. CIRCULATION 2013;127(2):213–223. [PubMed: 23224061]

59. Karantalis V, Suncion-Loescher VY, Bagno L, et al. Synergistic Effects of Combined Cell Therapy for Chronic Ischemic Cardiomyopathy. J. AM. COLL. CARDIOL 2015;66(18):1990–1999. [PubMed: 26516002]

Significance Statement:

hCPC biological function is hampered by limited expansion potential and early replicative senescence. Permanent hypoxia (1% O_2) preserved clonogenicity and mitochondrial function of hCPC derived from heart failure (HF) patients while maintaining high levels of intracellular NAD^+/NADH ratio and suppressing ROS and oxidative stress.

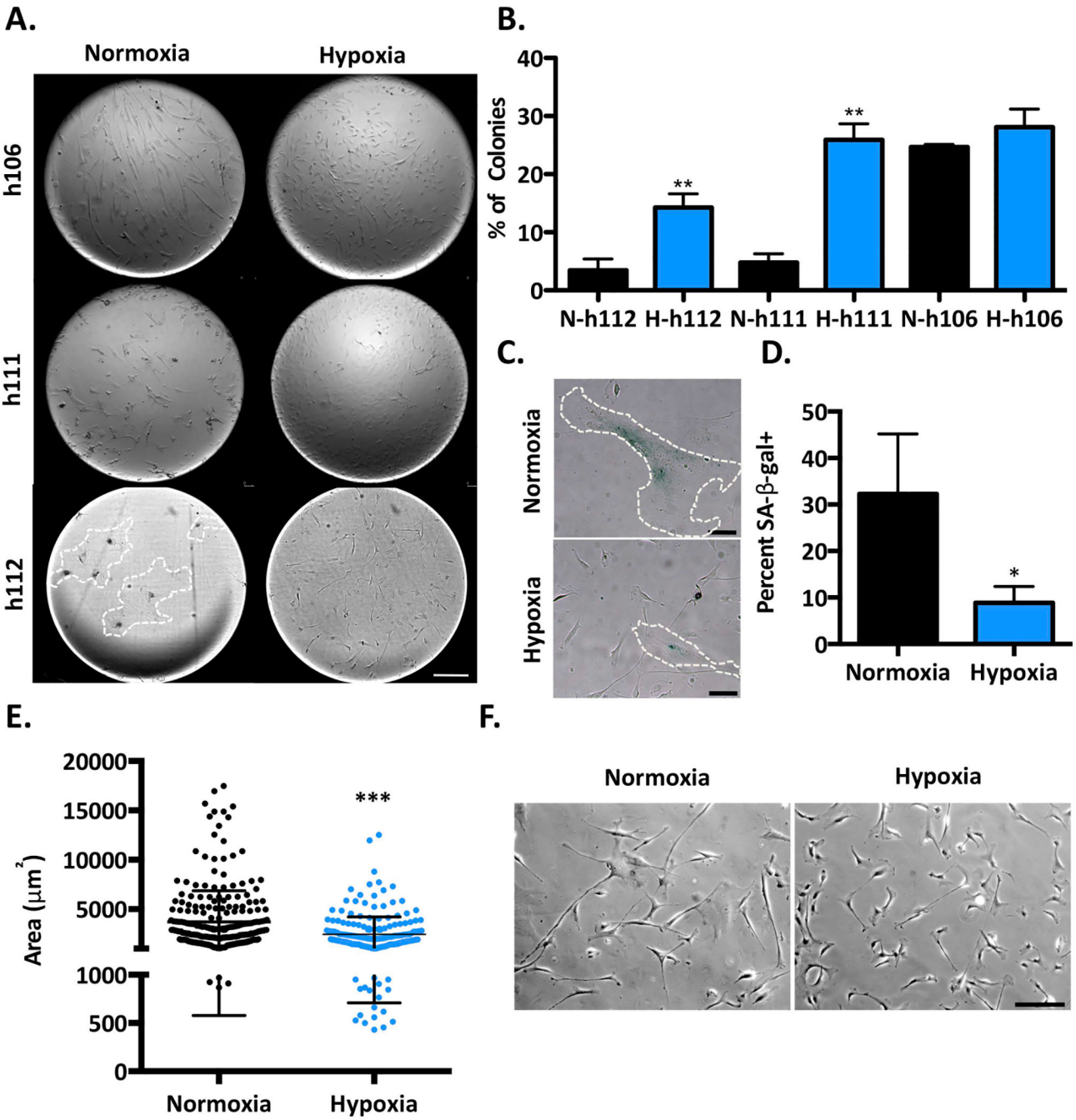

Figure 1. Long-term hypoxic culture enhances hCPC clonogenicity and delays senescence.

A. Representative images of colonies formed from single cells (1 cell/10μl) plated in 72-well Terazaki plates in hypoxia and normoxia. Scale bar = 250μm. **B**. Colony formation quantification. h112 N=4, h111 and h106 N=3. **C**. Senescence-associated β-galactosidase (SA-β-gal) staining and quantification (**D**.) of normoxic and hypoxic h112 hCPCs. Scale bar = 50μm. N=3. (**E**.) Morphological assessment of h112 hCPC-21% (normoxia) and hCPC-1% (hypoxia) over passages 4–6. (**F**.) Representative phase-contrast images of hCPCs. Scale bar 200μm. Mean± SD; *P<0.05, **P<0.01, ***P<0.001 vs. Normoxia.

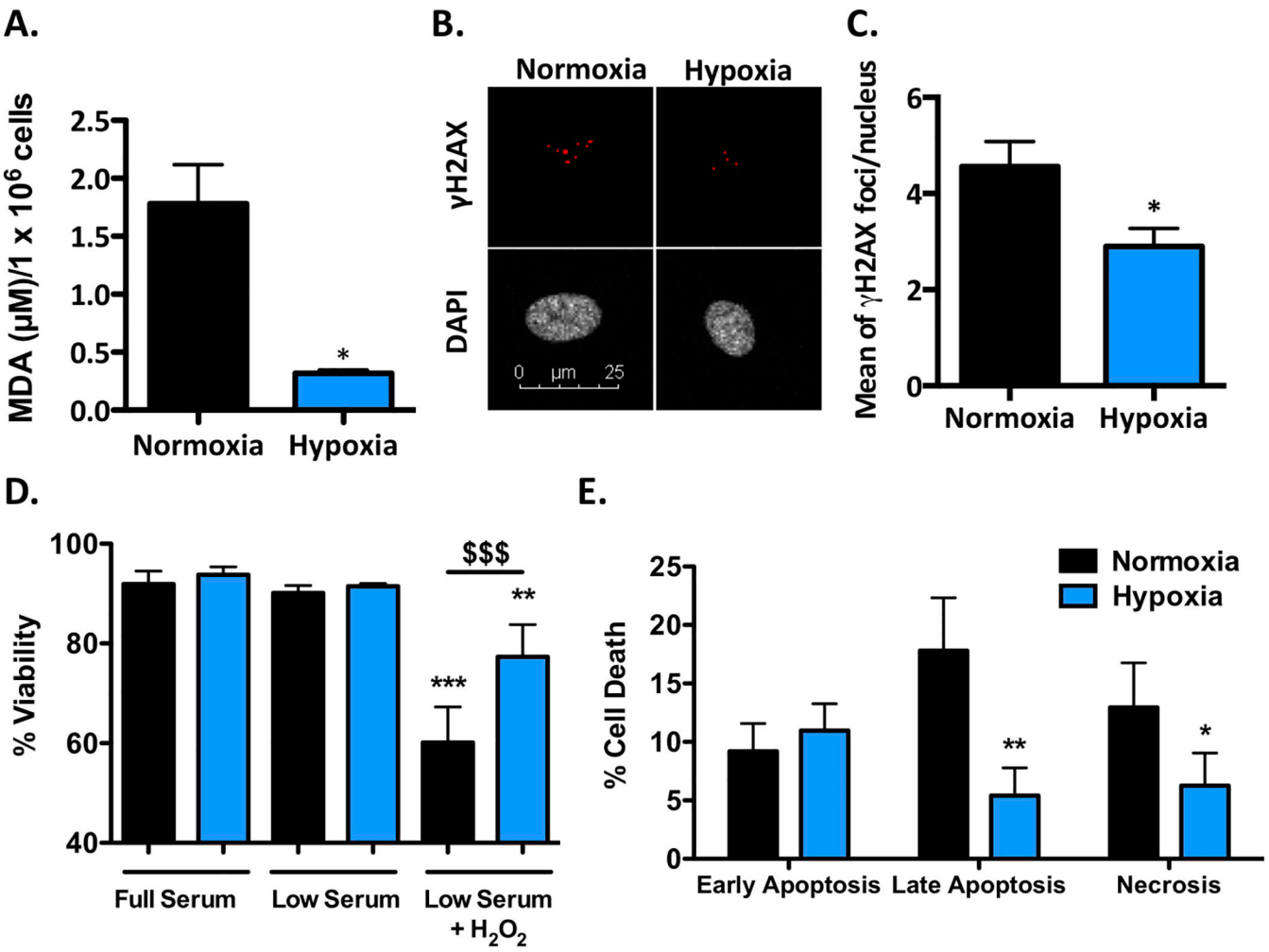

Figure 2. Oxidative stress is mitigated and resistance to cell death is enhanced by hypoxia in hCPCs.

(A) Malondialdehyde (MDA) quantification in normoxic (hCPC-21%) and hypoxic (hCPC-1%) hCPCs. N=3. (B) γH2AX staining and (C) quantification of untreated normoxic and hypoxic hCPCs. n=120 cells. (D) Percent viable cells after 4 hours treatment with 750 μM H_2O_2. (E) Percent apoptotic and necrotic cells after 4 hours of H_2O_2 treatment. N=3. Mean ± S.D.; *p < 0.05; **p<0.01; ***p<0.001 vs. Normoxia; $ $ $p<0.01

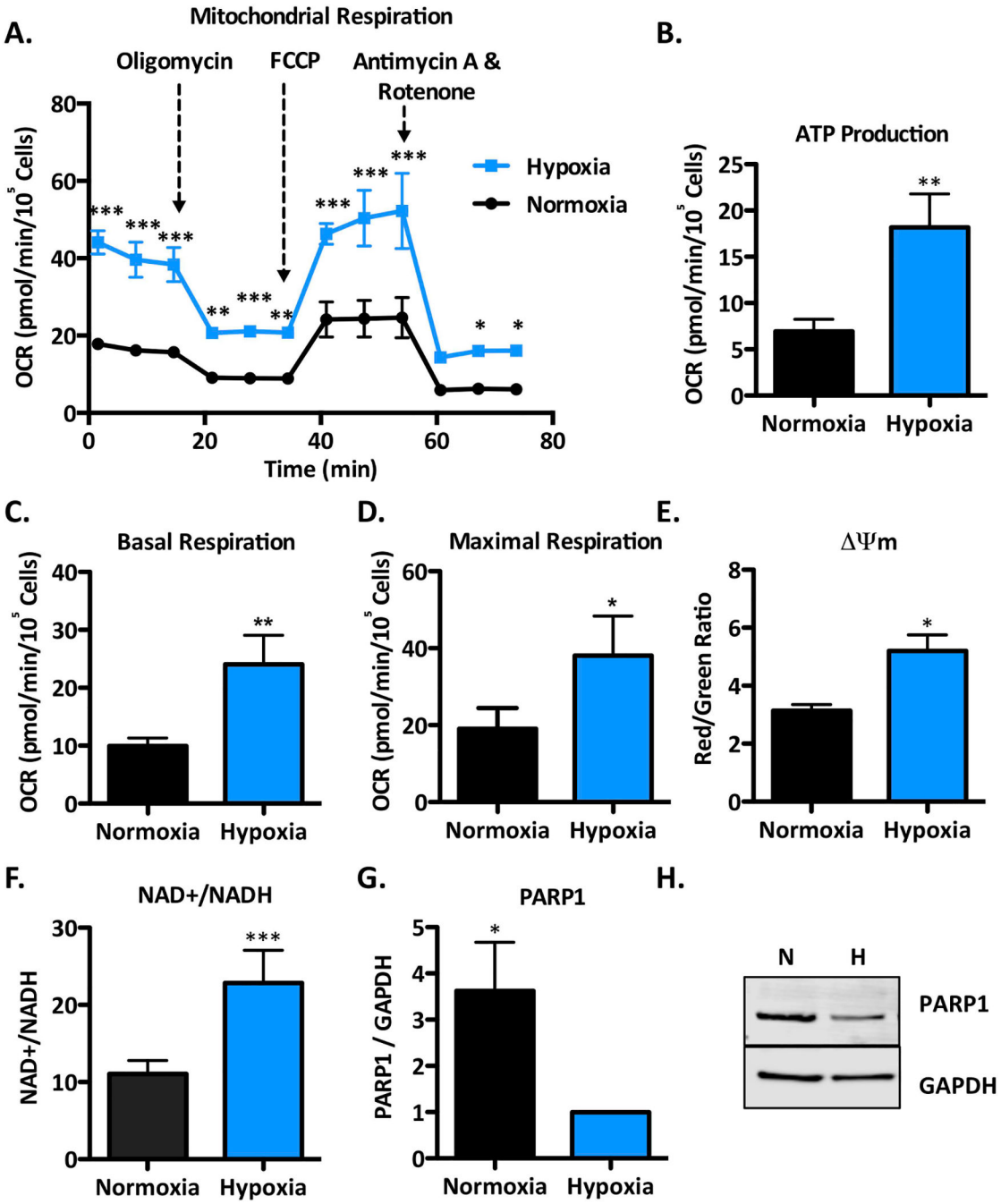

Figure 3. Mitochondrial function is preserved by hypoxia in hCPCs.

A. Mitochondrial oxygen consumption rate (OCR) of normoxic (hCPC-21%) and hypoxic (hCPC-1%) hCPCs. N=3. hCPC-1% had significantly higher ATP production-coupled OCR (**B**.), basal OCR **(C**.), and maximal uncoupled OCR (**D**.) compared to hCPC-21%. N=3. **E**. Mitochondrial membrane potential, measured by JC-1 red:green ratio, was significantly higher in hCPC-1% vs. hCPC-21%. N=3. **F**. NAD^+/NADH ratio was significantly higher, while expression of PARP1 was significantly lower (**G & H**) in hCPC-1%. N=3. Mean ± S.D., *P<0.05, **P<0.01, ***P<0.001 vs. Normoxia.

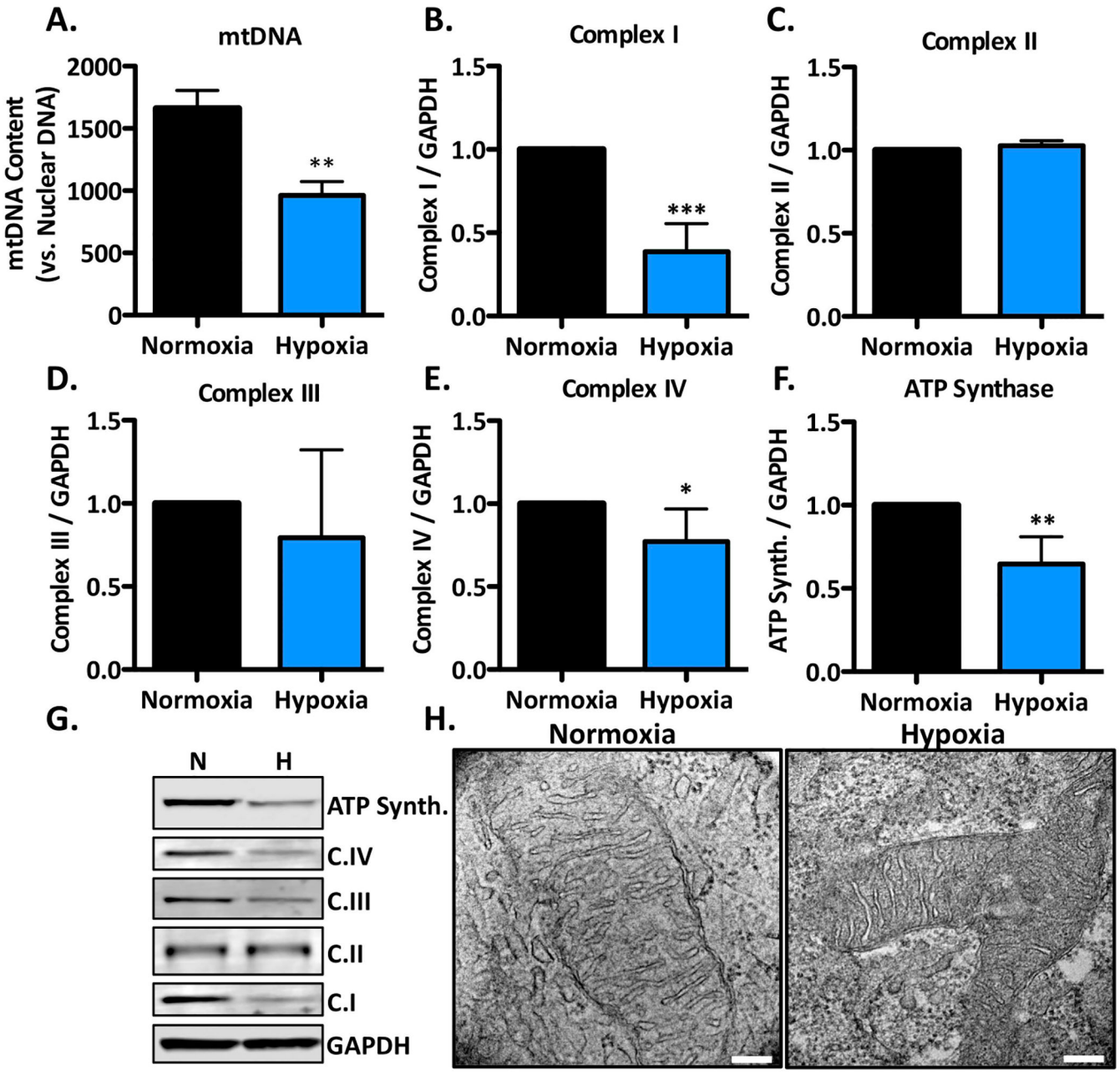

Figure 4. Mitochondrial content is decreased by hypoxic hCPC culture.

A. Mitochondrial DNA content relative to nuclear DNA. N=3. Quantification of subunits from electron transport complexes I **(B**.), II (**C**.), III **(D**.), IV **(E**.), and ATP Synthase **(F**.). N=3–6. Mean ± S.D. *P<0.05; **P<0.01; ***P<0.001. **G**. Representative immunoblot. **H**. Representative TEM micrographs of normoxic (hCPC-21%) and hypoxic (hCPC-1%) hCPCs at 67,000X magnification. Scale bar 200nm.

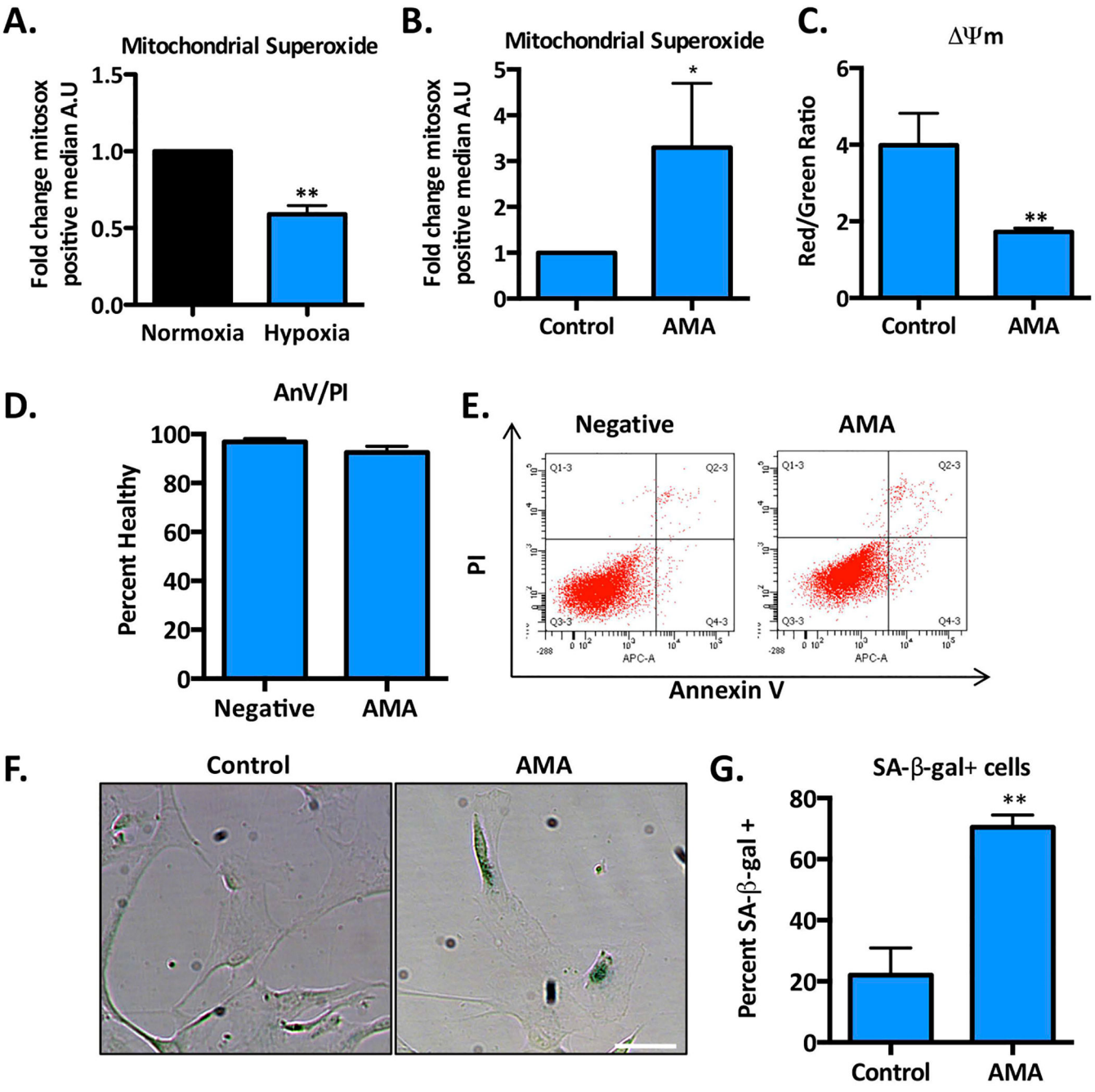

Figure 5. Mitochondrial ROS accelerates senescence in hCPCs.

A. Relative MitoSOX Red fluorescence intensity in hCPCs under basal normoxic and hypoxic culture conditions. N=3. **B**. MitoSOX Red fluorescence intensity of hCPC-1% treated with DMSO (Control) or 100 μM antimycin A for 9 days. N=4. **C**. Mitochondrial membrane potential (ΔΨm) measured by JC-1 red:green ratio using flow cytometry in hCPC-1% after 9 days AMA treatment. N=3. **D**. Percent viable cells after 48h AMA treatment, measured by AnnexinV/PI assay. N=3. **E**. Representative flow cytometry scatter plots of cell death assay. **F**. SA-β-gal staining and quantification Scale bar 200μm. (**G**.) following 9 days of AMA treatment. N=4. Mean ± SD., *p<0.05; **p<0.01.

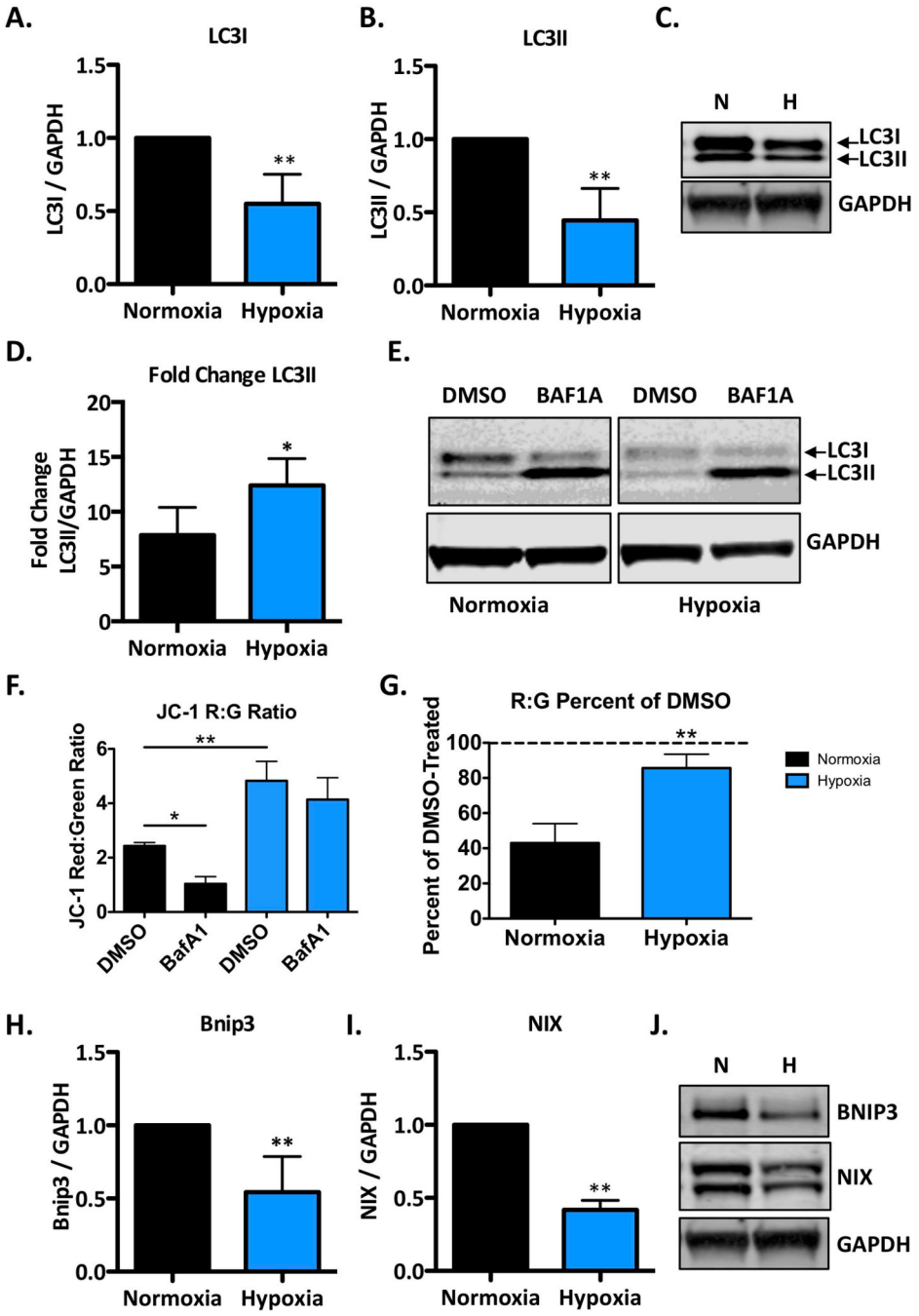

Figure 6. Mitophagy supports mitochondrial function in normoxic hCPCs.

Quantification of LC3I (**A**.), and LC3II (**B**.), with representative immunoblots (**C**.). N=3. Quantification (**D**.) and representative immunoblots (**E**.) of LC3II in bafilomycin A1 treated hCPCs. N=5. JC-1 red:green ratio (**F**.) and expressed as percent of DMSO-treated (**G**.) after 24 hours of DMSO or 50 nM bafilomycin A1 treatment. N=3. Protein expression levels of mitophagy receptors BNIP3 **(H.)** and NIX **(I**.), and representative blots (**J**.). N=3. "N" = normoxia, "H" = hypoxia. Mean ± SD.;*P<0.05, **P<0.01 vs. Normoxia.

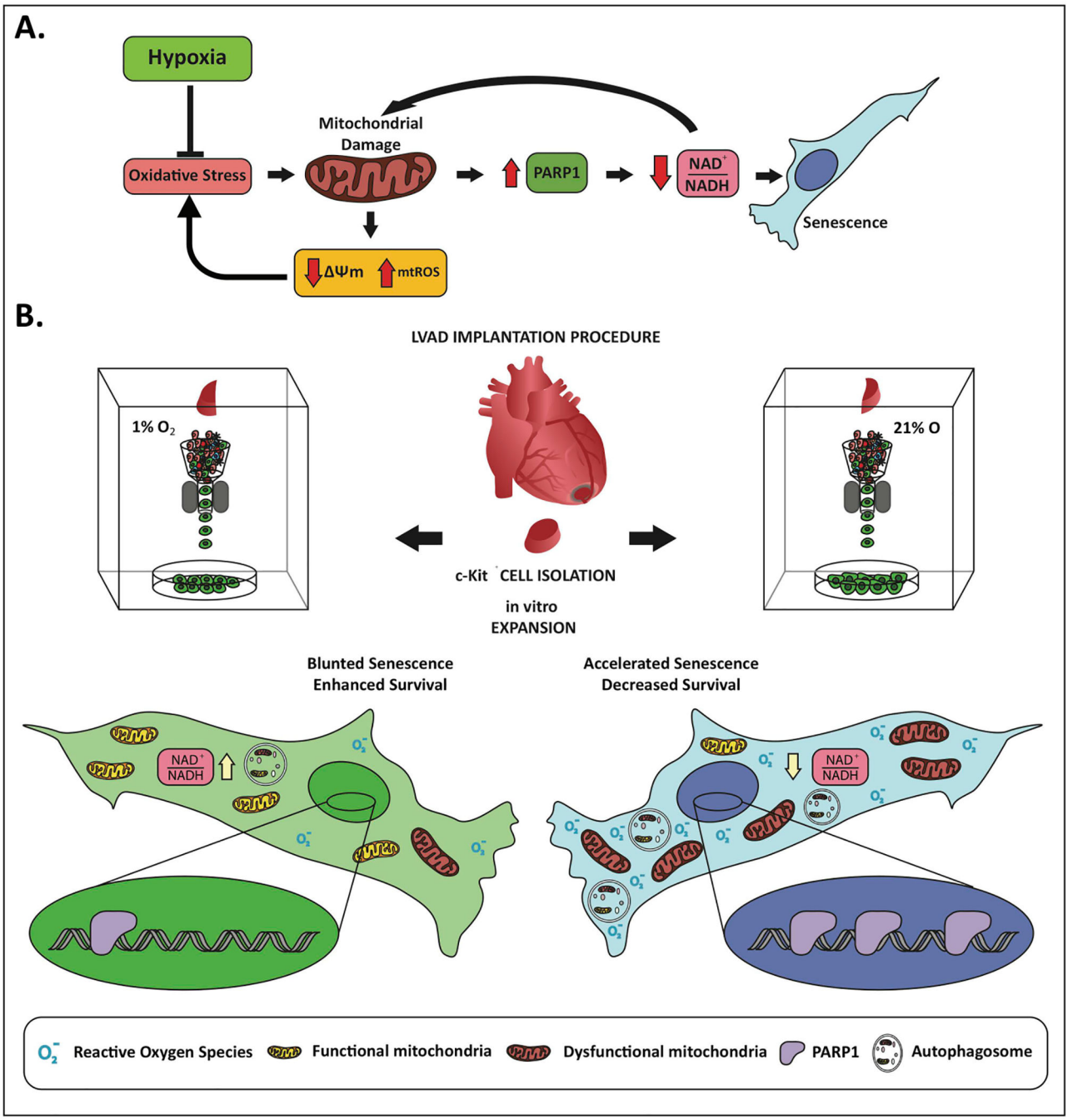

Figure 7. Long-term hypoxic culture preserves hCPC mitochondrial function and inhibits senescence.

(A) Schematic of feed-forward cycle of oxidative damage on hCPC-21% that leads to mitochondrial dysfunction and senescence in normoxic culture. The cycle is rescued by hypoxic culture of hCPCs. (B) Illustration of hypoxic and normoxic isolation and expansion strategies and respective outcomes on either hCPC-1% or hCPC-21%.

Table 1.

List of Primers

Gene	Forward Primer (5'-3')	Reverse Primer (5'-3')
mtDNA: tRNA-Leu(UUR)	CAC CCA AGA ACA GGG TTT GT	TGG CCA TGG GTA TGT TGT TA
nucDNA: B2-microglobulin	TGC TGT CTC CAT GTT TGA TGT ATC T	TCT CTG CTC CCC ACC TCT AAG T

Table 2.

List of Antibodies and Stains

Antibody/Stain	**Producer and catalog #**	**Application IB: Immunoblot; ICC: Immunocytochemistry; Flow**	**Dilution**
BNIP3	Sigma, catalog # B7931	IB	1:1000
GAPDH (Goat pAb)	Sicgen, catalog # AB0067–200	IB	1:1000
GAPDH (Mouse mAb)	Millipore, catalog # MAB374	IB	1:1000
LC3A/B	Cell Signaling Technology, catalog # 4108	IB	1:1000
BNIP3L (NIX)	Abcam, catalog # ab8399	IB	1:1000
Total OXPHOS Human Antibod Cocktail	Abcam, catalog # ab110411	IB	1:500
PARP (Rabbit mAb)	Cell Signaling Technology, catalog # 9532	IB	1:500
DAPI	Sigma, catalog # D8417	ICC	1:10,000
γH2A.X	Millipore, catalog # 05–636	ICC	1:500
LC3A	Novus Biologicals catalog # NBP1–19167)	ICC	1:300
MTCO1	Abcam, catalog #ab14705	ICC	1:300
c-KIT	R&D systems, catalog # AF1356	Flow	1:33
CD105	Biolegend, catalog # 323203	Flow	1:33
CD34	Santa Cruz, catalog # SC-9095	Flow	1:33
CD166	Abcam, catalog # ab109215	Flow	1:90

Table 3.

Patient Data

Line	Age	Gender	Hypertension	Smoking	Vessel disease
h106	62	M	yes	history of marijuana use	6 vessel coronary artery bypass graft
h111	61	M	yes	active smoker	single vessel artery disease
h112	46	M	yes	active smoker	mural thrombus